Available online at www.sciencedirect.com
ScienceDirect
Journal of Power Sources 178 (2008) 483–489
JOURNAL OF POWER SOURCES
www.elsevier.com/locate/jpowsour

Electrochemical properties of manganese oxide coated onto carbon nanotubes for energy-storage applications

Sang-Bok Ma [a], Kyung-Wan Nam [b], Won-Sub Yoon [b], Xiao-Qing Yang [b], Kyun-Young Ahn [c], Ki-Hwan Oh [d], Kwang-Bum Kim [a,*]

[a] *Department of Materials Science and Engineering, Yonsei University, 134 Shinchon-dong, Seodaemoon-gu, Seoul 120-749, South Korea*
[b] *Chemistry Department, Brookhaven National Laboratory, Upton, NY 11973, USA*
[c] *Hyundai ECO Technology Research Institute, Yongin-Si, Gyeonggi-Do 446-912, South Korea*
[d] *Next Generation Vehicle Technology, Seoul National University, Shinlim-dong, Kwanak-gu, Seoul 151-742, South Korea*

Received 6 August 2007; received in revised form 7 November 2007; accepted 3 December 2007
Available online 23 December 2007

Abstract

Birnessite-type manganese dioxide (MnO_2) is coated uniformly on carbon nanotubes (CNTs) by employing a spontaneous direct redox reaction between the CNTs and permanganate ions (MnO_4^-). The initial specific capacitance of the MnO_2/CNT nanocomposite in an organic electrolyte at a large current density of 1 A g^{-1} is 250 F g^{-1}. This is equivalent to 139 mAh g^{-1} based on the total weight of the electrode material that includes the electroactive material, conducting agent and binder. The specific capacitance of the MnO_2 in the MnO_2/CNT nanocomposite is as high as 580 F g^{-1} (320 mAh g^{-1}), indicating excellent electrochemical utilization of the MnO_2. The addition of CNTs as a conducting agent improves the high-rate capability of the MnO_2/CNT nanocomposite considerably. The in situ X-ray absorption near-edge structure (XANES) shows improvement in the structural and electrochemical reversibility of the MnO_2/CNT nanocomposite after heat-treatment.

Keywords: Manganese oxide; Carbon nanotube; Nanocomposite; Electrochemical capacitor

1. Introduction

Electrochemical capacitors (ECs) are energy-storage devices with a specific energy and specific power lying somewhere between batteries and conventional dielectric capacitors [1]. The applications of ECs include electric vehicles (EVs), uninterruptible power supplies (UPS), d.c. power systems, renewable energy and mobile devices. The ECs are classified into two types according to their charge storage principle [2]. The first is an electrical double-layer capacitor (EDLC) using activated carbon (AC) with high surface area and the other is a pseudocapacitor using metal oxides and conducting polymers.

The pseudocapacitance of a pseudocapacitor is the result of a capacitive relationship between the level of charge acceptance and the change in potential from a Faradaic redox reaction between the electrode material and electrolyte [3]. Among the various transition metal oxide materials used in pseudocapacitors, amorphous and hydrated ruthenium oxide has been reported to show a remarkably high specific capacitance (720 F g^{-1}) compared with other oxides [4,5]. However, its commercial use is limited by its expense. Therefore, considerable effort has been devoted to identifying alternative and inexpensive metal oxide electrode materials with acceptable electrochemical properties. Manganese dioxide (MnO_2) is one of the candidates on account of its electrochemical behaviour, low cost and environmental compatibility [6–11]. The pseudocapacitive properties of manganese oxide have been investigated mainly in aqueous solutions [6–20].

Recent studies of composite electrodes made from manganese oxide and carbonaceous materials have reported a high specific capacitance and rate capability of manganese oxide, particularly when a small amount of manganese oxide is dispersed uniformly over conductive and porous carbonaceous materials with a high surface area [12–26].

* Corresponding author. Tel.: +82 2 21232839; fax: +82 2 3125375.
E-mail address: kbkim@yonsei.ac.kr (K.-B. Kim).

0378-7753/$ – see front matter © 2008 Elsevier B.V. All rights reserved.
doi:10.1016/j.jpowsour.2007.12.027

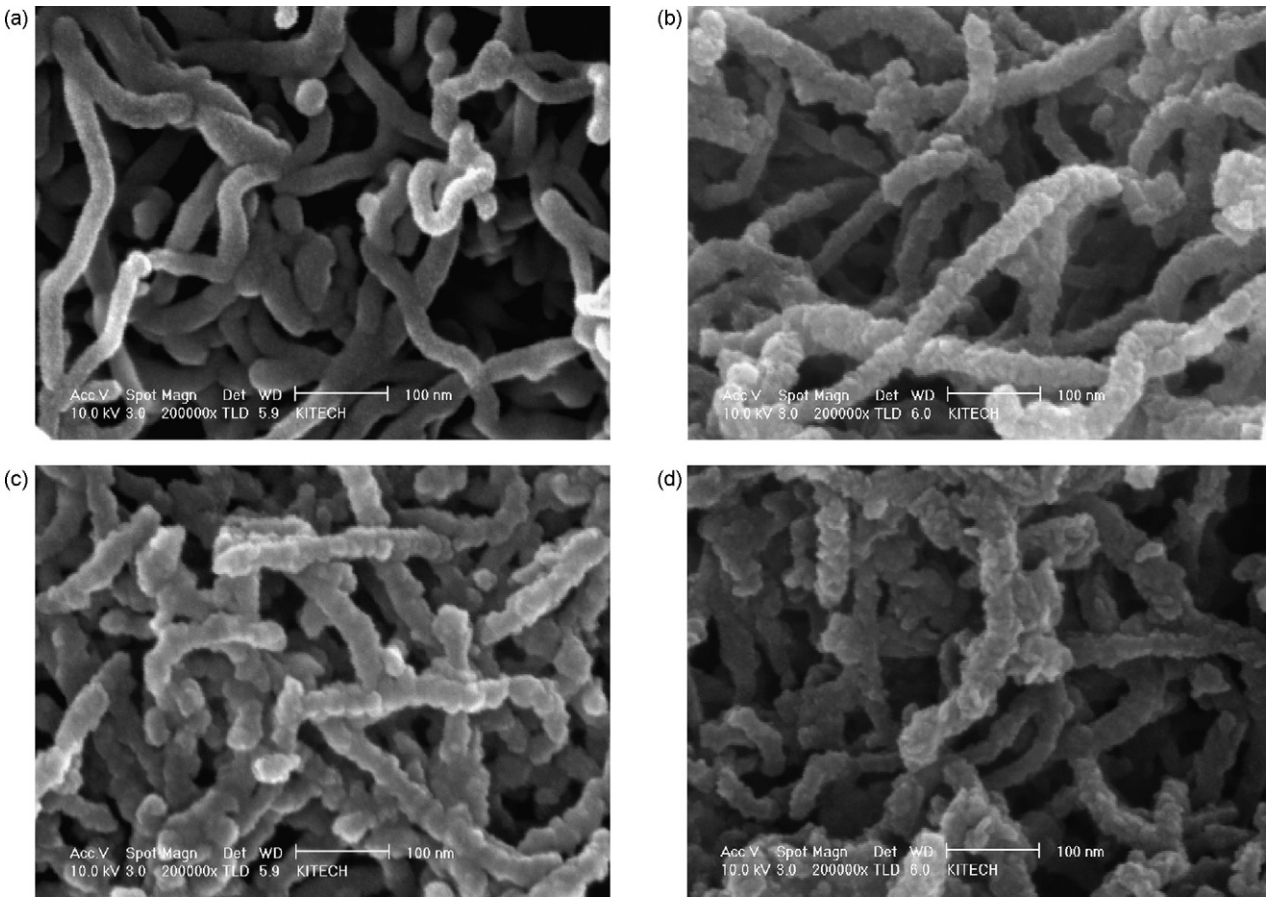

Fig. 1. SEM images of (a) pristine CNT and MnO_2/CNT nanocomposite prepared in 200 ml aqueous solution of 0.1 M $KMnO_4$ containing 1.0 g CNT at 70 °C under (b) pH 7; (c) pH 2.5; and (d) pH 1 of initial solution.

Carbon nanotubes (CNTs) have been studied extensively as electrode materials (100–200 F g^{-1}) for electrochemical capacitors [27,28], as additives for improving the electrode performance of metal oxides [12–16,29], and as deposition substrates for metal oxides in pseudocapacitors [17,18,30,31]. They have good chemical stability, good conductivity and a large surface area. In addition, CNTs are strongly entangled, which provides a network of open mesopores. Because the pseudocapacitive reaction of manganese oxide is a surface reaction, MnO_2/CNT composites with a nanometer-scale layer of manganese oxide are expected to show high specific capacity and good high-rate capability.

Previously, we reported the synthesis of composites of birnessite phase MnO_2 with acetylene black (AB) and CNTs for pseudocapacitor applications by direct spontaneous deposition [21,22]. This paper reports the electrochemical properties of MnO_2/CNT nanocomposites in 1 M $LiClO_4$ in propylene carbonate (PC) for pseudocapacitor applications. The structural and electrochemical reversibility of the MnO_2/CNT nanocomposite is examined by in situ X-ray absorption near-edge structure (XANES) analysis.

2. Experimental

Birnessite manganese dioxide was deposited on CNTs (multiwalled CNTs, ILJIN Nanotech, $S = 200\ m^2\ g^{-1}$) through a direct redox reaction between the CNTs and MnO_4^-. The detailed procedure for preparing the MnO_2/CNT nanocomposite is described elsewhere [22]. Briefly, 0.1 M $KMnO_4$ (99+%, Aldrich) solutions were heated to 70 °C, and 1.0 g of the as-received CNTs was then added to solutions at pH 1, 2.5 and 7, which was controlled by adding 0.01 M HCl. During synthesis, the solution temperature was maintained at 70 °C using a circulator. The suspension was filtered, washed several times with distilled water, and dried at 100 °C for 24 h in a vacuum oven. Herein, this product is referred to as the 'as-prepared MnO_2/CNT nanocomposite'. After drying, some of the products prepared at pH 7 were heat-treated at 200 °C for 24 h in a vacuum, and is referred to as the 'heat-treated MnO_2/CNT nanocomposite'.

Scanning electron microscopy (SEM, Sirion, FEI) was used to observe the morphology of the MnO_2/CNT nanocomposite powders. The electrochemical measurements were carried out with a three-electrode electrochemical cell, for which two lithium foils were used as the counter and reference electrodes, respectively. The working electrode consisted of a mixture of the MnO_2/CNT nanocomposite, a conducting agent and a binder. Either 28 wt.% CNT or acetylene black was used as the conducting agent, and 5 wt.% polyvinylidene fluoride (PVDF) dissolved in *N*-methylpyrrolidone served as the binder. A slurry of the mixture was coated on titanium foils, which was followed by drying at 100 °C for 12 h. Each working electrode with a 1 cm × 1 cm

area contained 1 mg of the dried slurry. The electrolyte was 1 M $LiClO_4$ in PC. Discharge and charge cycles were carried out between 1.5 and 3.5 V by means of a potentiostat/galvanostat (VMP2, PRINCETON APPLIED RESEARCH) at a current density of 1, 5 or 10 A g^{-1}, where the weight was based on the total electrode material which includes the electroactive material, conducting agent and binder.

The in situ Mn K-edge X-ray absorption spectra (XAS) were measured in transmission mode at the beamline X19A of the National Synchrotron Light Source (NSLS) using a Si(1 1 1) double-crystal monochromator that had been de-tuned to 35–45% of its original intensity to eliminate high order harmonics. Energy calibration was performed using the first inflection point of the spectrum of Mn metal foil as a reference (i.e., Mn K-edge = 6539 eV). The reference spectra were collected simultaneously for each in situ spectrum using a Mn metal foil. The detailed design of the spectroelectrochemical cell employed in the in situ XAS measurement has been described elsewhere [32].

3. Results and discussion

3.1. Morphology of MnO_2 coated onto CNT

A very thin MnO_2 layer was coated spontaneously on CNT substrates. Fig. 1 shows SEM images of the CNTs before and after MnO_2 deposition in a 200 ml aqueous solution of 0.1 M $KMnO_4$ with different initial pHs containing 1.0 g CNT at 70 °C. The mechanism for the synthesis of the MnO_2/CNT nanocomposite is described elsewhere [22]. Each CNT was approximately 20–30 nm in diameter, as shown in Fig. 1(a). After MnO_2 deposition, the diameter of the CNTs increased slightly to 30–50 nm, as shown in Fig. 1(b–d). It should be noted that none of the MnO_2 deposits blocked the opening of the three-dimensional entangled structure of the CNTs. The morphology of MnO_2 in the MnO_2/CNTs became rougher with decreasing pH of the initial solution. MnO_2 deposited on the CNTs at pH 1 (Fig. 1(d)) consisted of nano-scale MnO_2 while the layer deposited from the solution at pH 7 in Fig. 1(b) had a thin film form. This might be explained in terms of the faster reduction of MnO_4^- to MnO_2 at pH 1 than at pH 7 [22].

3.2. Electrochemical properties of MnO_2 coated on CNT

Fig. 2 shows the first discharge curves of the MnO_2/CNT nanocomposite prepared in the solution at pH 7. This electrode had AB as the conducting agent. The charge and discharge cycles were performed at current densities of 1, 5 and 10 A g^{-1}, where the weight is based on the total electrode weight including the electroactive material, conducting agent and binder. As shown in Fig. 2, the first discharge curves of the birnessite-type MnO_2/CNT composite showed no obvious plateau, which indicates a typical capacitive behaviour. The specific capacitance of the electrode was calculated from the discharge profile using the following equation:

$$C = \frac{I\,\Delta t}{V} \quad (1)$$

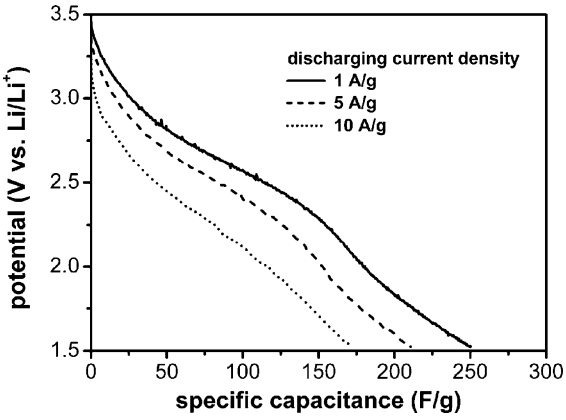

Fig. 2. Initial discharge profiles of MnO_2/CNT nanocomposite at different current densities, using AB as conducting agent in 1 M $LiClO_4$ in PC.

where: C (F g^{-1}) is the specific capacitance of the electrode; Δt (s) is the discharge time; V (V) is the potential range from the end of charge to the end of discharge; I (A g^{-1}) is the applied current density based on the total electrode material. The initial specific capacitance of the total electrode material, including the electroactive material, conducting agent and binder, is 250 F g^{-1} at a current density of 1 A g^{-1}, which is equivalent to 139 mAh g^{-1}. The specific capacitance per unit weight of the MnO_2/CNT composite is 370 F g^{-1}, which is equivalent to 207 mAh g^{-1}. Kawaoka et al. [26] reported the synthesis of MnO_2/Ketjen Black (KB) with a specific capacity of 165 mAh g^{-1}. The specific capacitance of the MnO_2 in the MnO_2/CNT composite is 580 F g^{-1}. This can be converted to 320 mAh g^{-1} for MnO_2 because the electrode contains 43 wt.% MnO_2. It should be noted that the specific capacitance of 580 F g^{-1} is measured at a high discharge rate of 1 A g^{-1} in 1 M $LiClO_4$ in PC. The theoretical specific capacity can be calculated from the following reaction:

$$MnO_2 + xLi^+ + xe^- \rightarrow Li_xMnO_2 \quad (2)$$

where: x is the number of moles of Li ions and electrons participating in the reaction. When 1 mol of Li ions and electrons participate in the reaction, the Mn(IV) in MnO_2 is reduced to Mn(III), and the theoretical specific capacity of MnO_2 is 308 mAh g^{-1}. Xu et al. [33] reported a specific capacity of 436 mAh g^{-1} for amorphous MnO_2 between 1.5 and 3.5 V (vs. Li/Li^+) in 1 M $LiClO_4$ in PC at a low current density of 20 μA cm^{-2}, which corresponds to 1.63 mol of Li^+ per mole of MnO_2. The specific capacitances of 211 and 171 F g^{-1} are achieved even at higher discharge current densities of 5 and 10 A g^{-1}, respectively, which indicates the very good high-rate capability of the MnO_2/CNT nanocomposite. The electrochemical properties of MnO_2 on the CNTs are attributed to the nanometer-scale coating of MnO_2 on the CNTs, the high interfacial area between the MnO_2 and electrolytic solution, and the interconnected pores in a three-dimensional entangled structure of CNTs.

3.3. Effect of initial solution pH

Fig. 3 shows the change in the specific capacitance of the MnO_2/CNT nanocomposites prepared in $KMnO_4$ solutions at

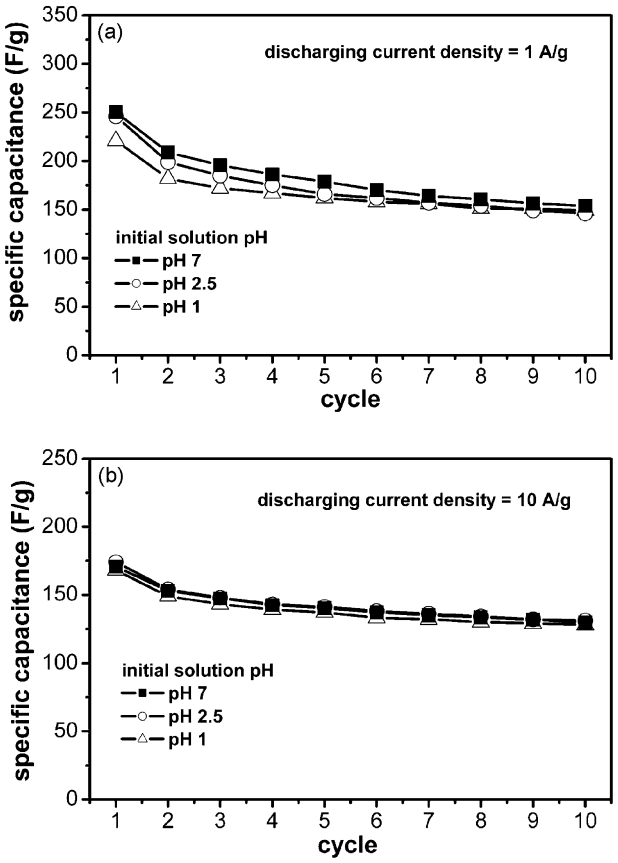

Fig. 3. Change in specific capacitance of MnO_2/CNT nanocomposite during cycling at (a) 1 A g^{-1} and (b) 10 A g^{-1}, using AB as conducting agent.

different initial pHs with initial cycling. As shown in Fig. 3(a), the initial specific capacitance of the MnO_2/CNT nanocomposite is 250 F g^{-1} at 1 A g^{-1} for the solution at pH 7, and decreases slightly as the initial pH of the $KMnO_4$ solution is changed from 7 to 1. The specific capacitance of all three MnO_2/CNT nanocomposites approaches 150 F g^{-1} at the tenth cycle regardless of the initial pH of the solution used for their preparation. At a high current density of 10 A g^{-1}, however, each of the MnO_2/CNT nanocomposites show an initial specific capacitance of approximately 171 F g^{-1}, and an identical decrease in specific capacitance during irrespective regardless of the initial pH, as shown in Fig. 3(b).

During discharge of the MnO_2/CNT nanocomposite electrode, the Mn(IV) in MnO_2 is reduced as lithium ions became intercalated into MnO_2. The diffusion length of lithium ions in MnO_2 can be determined using the following equation [25]:

$$L = (D\Delta t)^{1/2} \quad (3)$$

where: L (cm) is the lithium ion diffusion length; D (cm^2 s^{-1}) the solid-state diffusion coefficient of lithium in $Li_xMn_2O_4$; Δt (s) the discharge time. The calculated lithium diffusion length is approximately 30 nm considering the solid-state diffusion coefficient of lithium in $Li_xMn_2O_4$ to be 2.8×10^{-13} cm^2 s^{-1} [34] and a discharge time of 30 s at 10 A g^{-1}. The SEM images in Fig. 1 show that the thickness of MnO_2 on the CNTs is less than the lithium diffusion length of 30 nm, given the surface roughness of MnO_2 on the CNT prepared in solutions at different pHs. This suggests that all the MnO_2 coated on the CNTs in the three different MnO_2/CNT nanocomposites can participate in the electrochemical reaction, which leads to an identical discharge behaviour, as shown in Fig. 3. In addition, the surface roughness of MnO_2 on the CNTs is not large enough to change the electrochemical performance of the MnO_2/CNT nanocomposite.

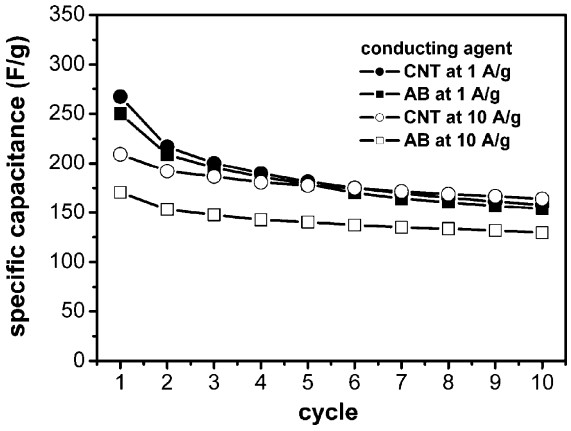

Fig. 4. Change in specific capacitance of MnO_2/CNT nanocomposite during cycling using either AB or CNT as conducting agent at 1 and 10 A g^{-1}.

3.4. Effect of CNT as a conducting agent

When AB is used as the conducting agent for the MnO_2/CNT nanocomposite electrode, the initial specific capacitance is approximately 250 F g^{-1} at a current density 1 A g^{-1}, as shown in Fig. 4. At 10 A g^{-1}, however, the specific capacitance decreases due to an increase in the ohmic drop with increasing current density. In order to improve the high-rate capability of the MnO_2/CNT nanocomposite electrode, the AB was replaced with CNT as the conducting agent in the preparation of the MnO_2/CNT nanocomposite electrode. In Fig. 4, MnO_2/CNT nanocomposite electrodes with CNT and AB as the conducting agent, respectively, exhibit similar electrochemical behaviour at 1 A g^{-1}. However, the initial specific capacitance of the MnO_2/CNT nanocomposite electrode is 210 F g^{-1} at 10 A g^{-1} for the CNTs, while it is 170 F g^{-1} for AB. Furthermore, the MnO_2/CNT nanocomposite electrode with CNT has a higher specific capacitance than the MnO_2/CNT nanocomposite electrode with AB during cycling, which indicates that the CNTs act more effectively in forming a conduction network in the composite electrode. This is because CNTs, as a conducting agent in the composite, have a long conduction path on the μm scale and provide many contact points with the MnO_2/CNT nanocomposites. This can further enhance the mesoporosity formed by the MnO_2/CNT nanocomposite and allow the easy access of ions [35].

3.5. Effect of heat-treatment of MnO_2/CNT nanocomposite

The specific capacitance of the MnO_2/CNT nanocomposite decreases from 250 to 160 F g^{-1} during cycling at 1 A g^{-1}, irre-

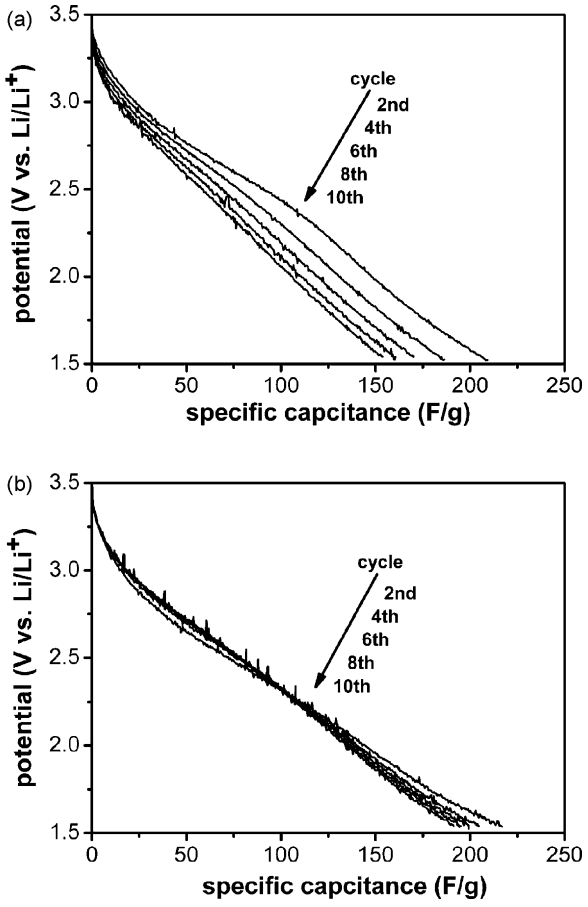

Fig. 5. Discharge profiles of (a) as-prepared and (b) heat-treated MnO_2/CNT nanocomposite during cycling.

spective of the conducting agent used (CNT or AB), as shown in Fig. 4. The degradation of MnO_2 results from changes in the composition and crystal structure of MnO_2 [36]. In this study, the MnO_2/CNT nanocomposite was heat-treated at 200 °C for 24 h in a vacuum to improve the cycleability of the MnO_2/CNT nanocomposite during charge–discharge cycles. Fig. 5 shows the discharge curves of the as-prepared and heat-treated MnO_2/CNT nanocomposite electrodes with the AB conducting agent during cycling at 1 A g^{-1}. The discharge capacitance of the as-prepared MnO_2/CNT nanocomposite decreases from 209 to 154 F g^{-1} after ten cycles, which indicates the rapid degradation of MnO_2, as shown in Fig. 5(a). There is, however, a slight change in the shape of the discharge curves with the heat-treated MnO_2/CNT nanocomposite during cycling, as observed in Fig. 5(b). The discharge capacitance of the heat-treated MnO_2/CNT nanocomposite decreases slightly from 217 to 191 F g^{-1} over ten cycles. The improved cycleability of the heat-treated MnO_2/CNT nanocomposite over the as-prepared MnO_2/CNT nanocomposite indicates its structural and chemical reversibility during repeated charge and discharge. This is consistent with the XANES results presented in Fig. 7.

Fig. 6 shows the normalized specific capacitance during cycling, which was obtained by dividing the specific capacitance at 1 A g^{-1} at each cycle by that obtained on the first cycle. For the as-prepared MnO_2/CNT nanocomposite, the normalized

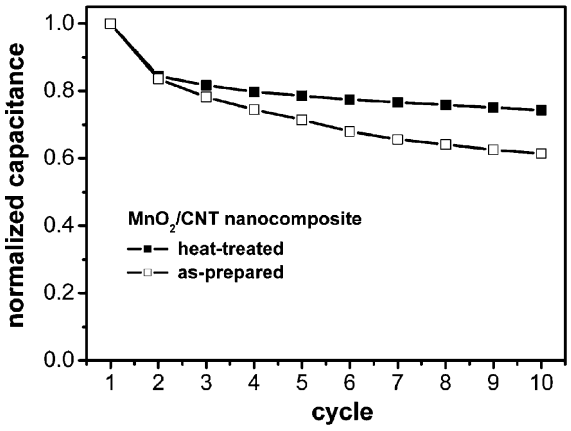

Fig. 6. Normalized capacitance of the as-prepared and heat-treated MnO_2/CNT nanocomposite during cycling.

ratio is 84% at the second cycle and 61% at the tenth, while it is 84 and 74% at the second and tenth cycle, respectively, for the heat-treated MnO_2/CNT nanocomposite.

Leroux et al. [37] reported the electrochemical behaviour of various layered manganese oxides. They found that interlayer water played a major role in the electrochemical behaviour of manganese oxides. In their study, dehydrated manganese oxides at $T > 200$ °C showed better retention over ten cycles and a larger Li^+ diffusion coefficient because of the decreased level of interlayer water. It is believed that, in this study, the improvement in cycleability by heat-treating the MnO_2/CNT nanocomposite is mainly due to dehydration of MnO_2 by heat-treatment [37,38].

3.6. In situ Mn K-edge XANES spectra of MnO_2/CNT nanocomposite

In order to determine the effect of heat-treatment on the structural stability of the MnO_2/CNT nanocomposite, a series of normalized in situ Mn K-edge XANES spectra were measured during charge–discharge cycles at a low current density of 44 mA g^{-1}. Fig. 7 shows the in situ Mn K-edge XANES spectra recorded after the as-prepared and heat-treated electrodes were charged to 4.0 V (vs. Li/Li^+) and discharged to 1.5 V (vs. Li/Li^+) during cycling. In all XANES spectra, there is a weak absorption peak (pre-edge) at ~6542 eV and a strong absorption peak at ~6560 eV. The weak pre-edge absorption is attributed to the electric dipole forbidden transition of a 1s electron to an unoccupied 3d orbital, which is partially allowed because of electric quadrupole coupling and/or 3d–4p orbital mixing arising from the noncentrosymmetric environment of the slightly distorted MnO_6 octahedral framework. The main absorption edge features near 6560 eV are assigned to the purely dipole-allowed $1s \rightarrow 4p$ transition [39]. Fig. 7 shows that charging the electrode to 4.0 V (vs. Li/Li^+) produces a shift in the absorption edge toward a higher energy, which implies an increase in the average oxidation state of the manganese ions in the electrode during charging. When discharged to 1.5 V (vs. Li/Li^+) for reduction, the absorption feature of the electrode shifts back to a lower energy, which indicates a decrease in the average oxidation state of the manganese ions in the electrode during discharging. The

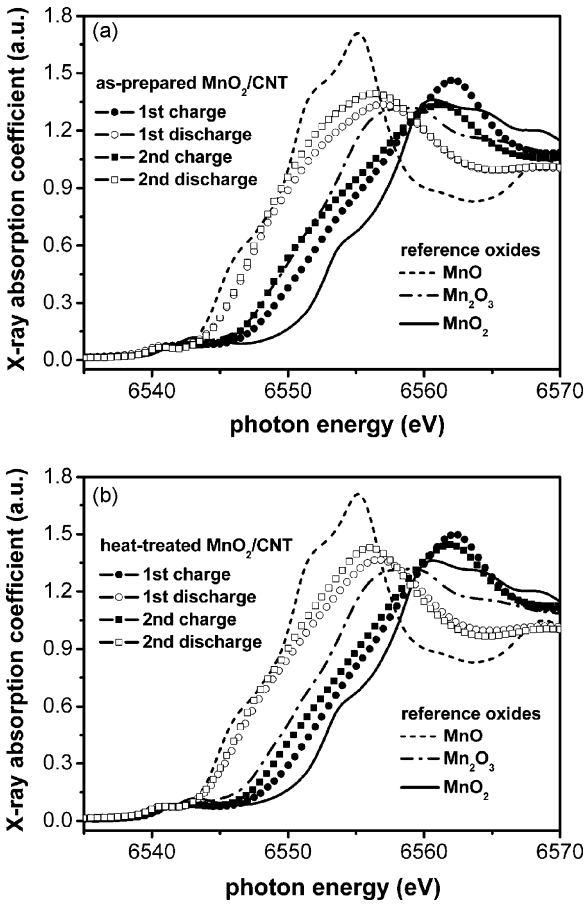

Fig. 7. In situ Mn K-edge XANES spectra of (a) as-prepared and (b) heat-treated MnO_2/CNT nanocomposite during cycling.

in situ XANES results of the MnO_2/CNT nanocomposites show that the electrochemical reaction of the MnO_2/CNT nanocomposite electrode during charge–discharge at a constant current is not due to double-layer charging by the CNTs, but to the Faradaic redox reaction between MnO_2 and Li^+ accompanied by a concomitant change in the oxidation state of Mn ions. This confirms that the reaction given in Eq. (2) represents the electrochemical reaction of the MnO_2/CNT nanocomposite.

In order to estimate the oxidation state of Mn in the MnO_2/CNT nanocomposite at the charged and discharged states, the XANES spectra for the MnO_2/CNT nanocomposite are compared with several reference oxides such as MnO (Aldrich), Mn_2O_3 (Aldrich) and MnO_2 (Aldrich). The XANES spectra for the charged MnO_2/CNT electrode are located between the XANES spectra for Mn_2O_3 (dash dot line) and MnO_2 (solid line), while the XANES spectra for the discharged MnO_2/CNT electrode are located between MnO (short dash) and Mn_2O_3 (dash dot line). Therefore, the oxidation state of Mn in the charged MnO_2/CNT nanocomposites is between 3+ and 4+, and that for the discharged MnO_2/CNT nanocomposites is between 2+ and 3+. It is well known that manganese oxides have various phases with different structures and oxidation states. Manganese oxides may have different XANES features even for the same oxidation state of Mn. Accordingly, it is difficult to extract the oxidation state of Mn from the XANES spectra for MnO_2/CNT nanocomposites in Fig. 7. Nevertheless, the XANES spectra provide qualitative and quasi-quantitative information by which the change in oxidation state can be estimated.

As shown in Fig. 7(a), the XANES features for the second charged states (-■-) of the as-prepared MnO_2/CNT nanocomposite do not shift back to the first charged state (-●-). This suggests that the change in the oxidation state of manganese ions as a result of the insertion–extraction of lithium ions is irreversible during charge–discharge. It is possible that not all the lithium ions inserted into the MnO_2 structure during the first discharging step are extracted in the second charging step.

On the other hand, the XANES feature at the second charged states of the heat-treated MnO_2/CNT nanocomposite shift back to the first charged state, as shown in Fig. 7(b). The heat-treated MnO_2/CNT nanocomposite has a higher absorption edge than that for the as-prepared MnO_2/CNT nanocomposite, which corresponds to a higher specific capacity of the heat-treated MnO_2/CNT nanocomposite during the second discharge. This indicates that the electrochemical redox reaction of the heat-treated MnO_2/CNT nanocomposite through the insertion–extraction of lithium ions is more reversible, which leads to better cycleability than the as-prepared one.

Further work analyzing the XANES data and extended X-ray absorption fine structure (EXAFS) of the MnO_2/CNT nanocomposites as well as evaluating the electrochemical behaviour during cycle is currently underway.

4. Conclusions

A nanometer-scale thick birnessite phase MnO_2 layer is deposited spontaneously on CNTs through the simple immersion of CNTs into an aqueous $KMnO_4$ solution. The initial specific capacitance of the MnO_2/CNT nanocomposite is approximately 250 F g^{-1} at a large current density of 1 A g^{-1}. This is equivalent to 139 mAh g^{-1} based on the total weight of the electrode material including the electroactive material, conducting agent and binder. The specific capacitance of MnO_2 in the MnO_2/CNT nanocomposite is as high as 580 F g^{-1} of MnO_2, which can be converted to 320 mAh g^{-1} of MnO_2. In addition, CNTs as a conducting agent enhances the high-rate capability of the MnO_2/CNT nanocomposite. The surface roughness of the MnO_2 on CNT increases with decreasing initial solution pH. By contrast, the pH of the initial solution has little influence on the electrochemical behaviour of the MnO_2/CNT nanocomposite. In situ Mn K-edge XANES analysis confirms that the structural and electrochemical reversibility of the MnO_2/CNT nanocomposite has been improved by heat-treatment.

Acknowledgement

This work was financially supported by the Ministry of Education and Human Resources Development (MOE), the Ministry of Commerce, Industry and Energy (MOCIE), and the Ministry of Labor (MOLAB) through the fostering project of the Lab of Excellency and by the ERC program of MOST/KOSEF (grant no. R11-2002-102-00000-0) and by Hyundai-Kia Motors and NGV.

References

[1] B.E. Conway, Electrochemical Supercapacitors; Scientific Fundamentals and Technological Applications, Kluwer Academic/Plenum, New York, 1999, pp. 11–13 (Chapter 2).
[2] B.E. Conway, J. Electrochem. Soc. 138 (1991) 1539–1548.
[3] B.E. Conway, Electrochemical Supercapacitors; Scientific Fundamentals and Technological Applications, Kluwer Academic/Plenum, New York, 1999, pp. 221–257 (Chapter 10).
[4] J.P. Zheng, T.R. Jow, J. Electrochem. Soc. 142 (1995) L6–L8.
[5] R. Kotz, M. Carlen, Electrochim. Acta 45 (2000) 2483–2498.
[6] H.Y. Lee, J.B. Goodenough, J. Solid State Chem. 144 (1999) 220–223.
[7] S.C. Pang, M.A. Anderson, T.W. Chapman, J. Electrochem. Soc. 147 (2000) 444–450.
[8] Y.U. Jeong, A. Manthiram, J. Electrochem. Soc. 149 (2002) 1419–1422.
[9] M. Toupin, T. Brousse, D. Belanger, Chem. Mater. 14 (2002) 3946–3952.
[10] C.C. Hu, T.W. Tsou, Electrochem. Commun. 4 (2002) 105–109.
[11] R.N. Reddy, R.G. Reddy, J. Power Sources 124 (2003) 330–337.
[12] Y.T. Wu, C.C. Hu, J. Electrochem. Soc. 151 (2004) 2060–2066.
[13] Y.K. Zhou, B.L. He, F.B. Zhang, H.L. Li, J. Soild State Electrochem. 482 (2004) 482–487.
[14] G.X. Wang, B.L. Zhang, Z.L. Yu, M.Z. Qu, Solid State Ionics 176 (2005) 1169–1174.
[15] E. Raymundo-Pinero, V. Khomenko, E. Frackowiak, F. Beguin, J. Electrochem. Soc. 152 (2005) A229–A235.
[16] V. Subramanian, H. Zhu, B. Wei, Electrochem. Commun. 8 (2006) 827–832.
[17] C.Y. Lee, H.M. Tsai, H.J. Chuang, S.Y. Li, P. Lin, T.Y. Tseng, J. Electrochem. Soc. 152 (2005) A716–A720.
[18] Z. Fan, J. Chen, M. Wang, K. Cui, H. Zhou, Y. Kuang, Diam. Relat. Mater. 15 (2006) 1478–1483.
[19] M. Wu, G.A. Snook, G.Z. Chen, D.J. Fray, Electrochem. Commun. 6 (2004) 499–504.
[20] A.E. Fischer, K.A. Pettigrew, D.R. Rolison, R.M. Stroud, J.W. Long, Nano Lett. 7 (2007) 281–286.
[21] S.B. Ma, Y.H. Lee, K.Y. Ahn, C.M. Kim, K.H. Oh, K.B. Kim, J. Electrochem. Soc. 153 (2006) C27–C32.
[22] S.B. Ma, K.Y. Ahn, E.S. Lee, K.H. Oh, K.B. Kim, Carbon 45 (2007) 375–382.
[23] H. Kawaoka, M. Hibino, H. Zhou, I. Honma, J. Power Sources 125 (2004) 85–89.
[24] M. Hibino, H. Kawaoka, H. Zhou, I. Honma, Electrochim. Acta 49 (2004) 5209–5216.
[25] H. Kawaoka, M. Hibino, H. Zhou, I. Honma, Solid State Ionics 176 (2005) 621–627.
[26] H. Kawaoka, M. Hibino, H. Zhou, I. Honma, Electrochem. Solid-State Lett. 8 (2005) A253–A255.
[27] C. Niu, E.K. Sichel, R. Hoch, D. Moy, H. Tennet, Appl. Phys. Lett. 70 (1997) 1480–1482.
[28] E. Frackowiak, K. Metenier, V. Bertagna, F. Beguin, Appl. Phys. Lett. 77 (2000) 2421–2423.
[29] J.S. Sakamoto, B. Dunn, J. Electrochem. Soc. 149 (2002) A26–A30.
[30] K.W. Nam, E.S. Lee, J.H. Kim, Y.H. Lee, K.B. Kim, J. Electrochem. Soc. 152 (2005) A2123–A2129.
[31] I.H. Kim, J.H. Kim, K.B. Kim, Electrochem. Solid-State Lett. 8 (2005) A369–A372.
[32] M. Balasubramanian, X. Sun, X.Q. Yang, J. McBreen, J. Power Sources 92 (2001) 1–8.
[33] J.J. Xu, A.J. Kinser, B.B. Owens, W.H. Smyrl, Electrochem. Solid-State Lett. 1 (1998) 1–3.
[34] E. Deiss, D. Haringer, P. Novak, O. Hass, Electrochim. Acta 46 (2001) 4185–4196.
[35] C. Portet, P.L. Taberna, P. Simon, E. Flahaut, J. Power Sources 139 (2005) 371–378.
[36] R. Chen, M.S. Whittingham, J. Electrochem. Soc. 144 (1997) L64–L67.
[37] F. Leroux, D. Guyomard, Y. Piffard, Solid State Ionics 80 (1995) 307–316.
[38] M.M. Thackeray, Prog. Solid State Chem. 25 (1997) 1–71.
[39] K.W. Nam, M.G. Kim, K.B. Kim, J. Phys. Chem. C 111 (2007) 749–758.